Performance of a double sided silicon strip detector as a transmission detector for heavy ions*

HAN Jian-Long(韩建龙)[1;1)] MA Jun-Bing(马军兵)[1] CAO Xi-Guang(曹喜光)[2] WANG Qi(王琦)[1]
WANG Jian-Song(王建松)[1] YANG Yan-Yun(杨彦云)[1;3] MA Peng(马朋)[1] HUANG Mei-Rong(黄美容)[1]
JIN Shi-Lun(金仕纶)[1;3] RONG Xin-Juan(戎欣娟)[1] BAI Zhen(白真)[1;3] FU Fen(付芬)[1]
HU Qiang(胡强)[1;3] CHEN Ruo-Fu(陈若富)[1] XU Shi-Wei(许世伟)[1] CHEN Jiang-Bo(陈江波)[1;3]
JIN Lei(金磊)[1;3] LI Yong(李勇)[1;3] ZHAO Ming-Hui(赵明辉)[1;3] XU Hu-Shan(徐瑚珊)[1]

[1] Institute of Modern Physics(IMP), Chinese Academy of Sciences(CAS), Lanzhou 730000, China
[2] Shanghai Institute of Applied Physics(SINAP), Chinese Academy of Sciences, Shanghai 201800, China
[3] University of Chinese Academy of Sciences, Beijing 100049, China

Abstract: The performance of a double sided silicon strip detector (DSSSD), which is used for the position and energy detection of heavy ions, is reported. The analysis shows that although the incomplete charge collection (ICC) and charge sharing (CS) effects of the DSSSD give rise to a loss of energy resolution, the position information is recorded without ambiguity. Representations of ICC/CS events in the energy spectra are shown and their origins are confirmed by correlation analysis of the spectra from both the junction side and ohmic side of the DSSSD.

Key words: charge sharing effect, incomplete charge collection, interstrip surface effect

PACS: 29.40.Gx **DOI:** 10.1088/1674-1137/38/5/056202

1 Introduction

The use of double sided silicon strip detectors (DSSSD) has become increasingly widespread over the past few decades as manufacturing techniques and reliability have been improved [1]. DSSSDs with a numbers of strips have been widely used in the detection of radioactive heavy ions, profiting from their high performance in energy and spacial resolution, and the covering of a large solid angle at the same time [2, 3]. Several detector systems with DSSSD arrays have been built for experimental research in the fields of radioactive beam physics and nuclear astrophysics, such as CD [2], LEDA [3], MUST [4] and DRAGON [5].

Silicon strip detectors rely on a high quality SiO_2 layer that is grown on the silicon [6, 7] to separate the finely segmented electrodes fabricated by doping the silicon. The SiO_2 separation area (i.e. the interstrip region of the detector) will induce incomplete charge collection (ICC) and charge sharing (CS) effects. These effects have been studied in large area single sided silicon strip detectors [8, 9] and segmented silicon sensors [10]. This paper reports some characteristics of ICC and CS effects of a DSSSD working in transmission mode for heavy ion beams.

In this investigation, the DSSSD is used as a transmission detector to detect the position and energy loss of heavy ions from an elastic scattering experiment [11, 12]. The origination of the ICC and CS evnets are confirmed, and the energy and position determination of these events are evaluated. This investigation is helpful for the data analysis of the extraction of elastic scattering events and their position information [11].

Section 2 briefly describes the DSSSD and the associated electronics. Section 3 is devoted to a description and analysis of the test result with ^{241}Am α source. The response of the DSSSD for highly ionising transmitting particles is discussed in Section 4. Conclusions are drawn in Section 5.

2 Experimental procedure

The DSSSD used for this investigation is an oxide passivated, ion-implanted, n-type silicon strip detector manufactured by EURISYS MESURES (type IPS48x48-150NxNy48). It consists of 48 aluminium strips of 0.9 mm width and 0.1 mm SiO_2 separations on junction (p^+) side, and 0.8 mm width strips with 0.2 mm sep-

Received 28 June 2013
* Supported by National Natural Science Foundation of China (10905076, 11005127, 11075190, 11205209, 11205221) and National Basic Research Program of China (973 Program) (2014CB845405)
1) E-mail: hanjl@impcas.ac.cn

arations on ohmic (n^+) side. Junction and ohmic side strips are orthogonal, providing effective pixel areas of $\sim$0.72 mm^2. The thickness of the detector is 150 μm. A perspective drawing of the DSSSD is shown in Fig. 1.

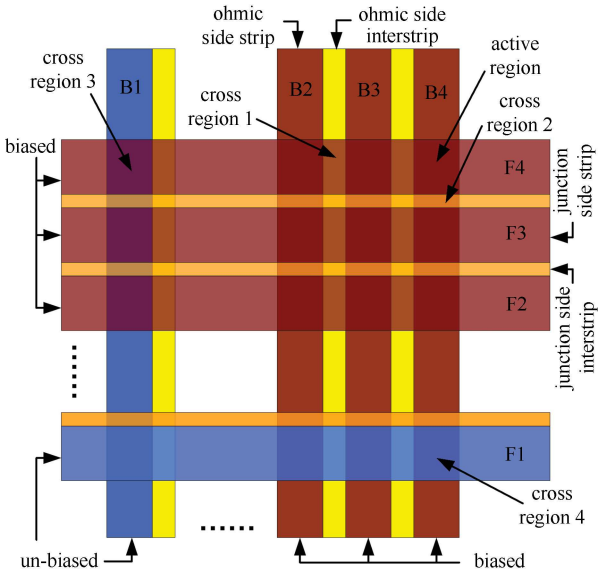

Fig. 1. Perspective drawing of the DSSSD, not in scale. The junction side faces to the reader. The biased and un-biased strips correspond to the test situation with a ^{241}Am α source, and all of the junction and ohmic side strips are biased for the test with heavy ion beams. The active region represents the normal working pixels of biased junction side strips cover biased ohmic side strips. Cross region 1 represents the areas of junction side strips cover ohmic side interstrips. Cross region 2 represents the areas of junction side interstrips cover ohmic side strips. Cross region 3 represents the areas of biased junction side strips cover un-biased ohmic side strips. Cross region 4 represents the areas of un-biased junction side strips cover biased ohmic side strips. See context for details.

In order to study the response of the DSSSD, the entire area of the junction side was illuminated using an ^{241}Am α source firstly, and then with heavy ion beams produced by the Radioactive Ion Beam Line in Lanzhou (RIBLL) [13] with energies which can punch through the DSSSD.

Figure 2 displays the block diagram of the front-end electronics. For the test with α source (offline test) 16 adjacent strips on both sides of the DSSSD are connected to the front-end electronics. These 16 junction side strips are biased to the advised operation voltage of -20 V referring to the user manual, and the ohmic side strips are earthed. The logical OR signal of the 16 junction side strips' signals is used as the gate/trigger signal of the standard CAMAC acquisition system (ACQ). For our investigation with heavy ion beams (online test) all of the strips of the DSSSD are biased to their full depletion voltage. A 1500 μm-thick single silicon detector (SSD) with effective area of 50 mm×50 mm is used to stop the penetrating particles from the DSSSD. The DSSSD and the SSD together work as a ΔE-E telescope. The gate/trigger signal for the ACQ comes from the SSD. Energy spectra of the single events from each strip are recorded, along with the spectra of any pulses that have occurred in coincidence in both adjacent strips.

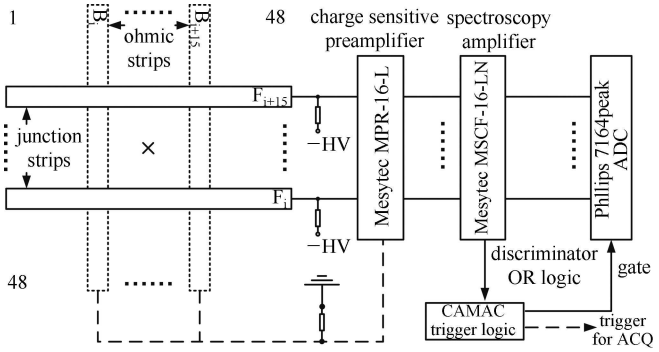

Fig. 2. Block diagram of the front-end electronics. × means the particles illuminate the DSSSD from the junction side.

3 Results of the offline test and analysis

The junction side of the DSSSD is illuminated by using an ^{241}Am radioactive source emitting 5.48 MeV α-particles. The responses of the junction and ohmic side strips are reported in this section. ICC and CS effects, which originate from the interstrip region of the DSSSD on both junction and ohmic sides, are analyzed.

3.1 α-particles' energy spectrum and the CS effect of the junction side strips

Figure 3(a) shows a spectrum collected from one junction side strip (for example the strip F4 in Fig. 1). Three sharp peaks are visible, in addition to a continuous background. The total energy peak (peak1 in Fig. 3(a)) corresponds to the 5.48 MeV α-particles stopped in the active region of the strip. For the active region, the corresponding junction and ohmic side strips are all connected to front-end electronics, and hence the normal circuit and electric field is built in the pixel region. The full width at half maximum (FWHM) of the total energy peak (i.e. the resolution of the energy measurement taken from the junction side strip of the DSSSD) is $\sim$45 keV. Peak3 and the continuous background are induced by the electron trapping effect [4, 8, 10, 14], which results in pulse height deficits of the α-particles stopped in the junction side interstrip regions. The ratio of the number of the counts in the peak3 and the continuous background to the counts

in the whole spectrum is about 10%. This ratio is consistent with the geometrical ratio between the area of the interstrip and strip regions on junction side.

The surprising thing is the appearance of peak2 that located near to the total energy peak. Peak2 will disappear if all of the junction and ohmic side strips are biased. Correlation analysis of peak2 with the ohmic side spectrum is performed to determine its origin. Events in peak2 are used as a restrictive cut (indicated by two up on end arrows in Fig. 3(a)) to inspect the corresponding spectrum of ohmic side strips. The result is shown in Fig. 3(b), it is clear that almost all of the events in peak2 correspond to the low channel noise signals of the ohmic side strip. The ratio of the number of counts in peak2 to the counts of peak2 add peak1 is about 70%. The ratio and the result of the correlation analysis lead to a conclusion that the peak2 is due to α-particles penetrating the DSSSD from cross region 3 (see Fig. 1), for which only the junction strips are connected to the front-end electronics during the offline test, while the area of cross region 3 occupies $2/3\approx70\%$ of the 16 junction side strips.

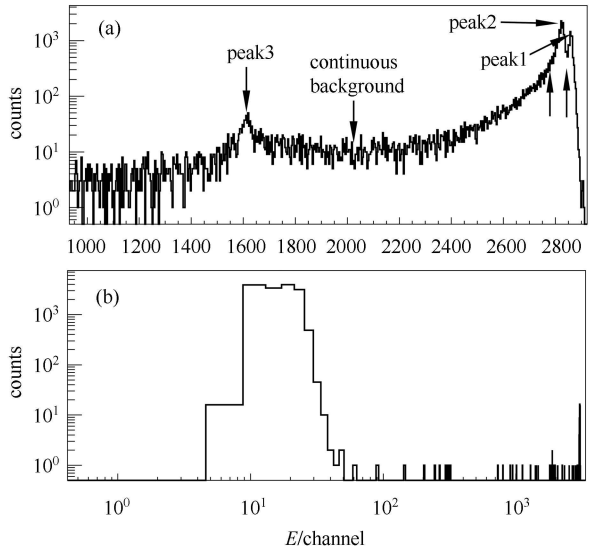

Fig. 3. (a) ^{241}Am α-particles' energy spectrum from one junction side strip. (b) The energy spectrum of one ohmic side strip corresponding to the selected peak2 as indicated by the two up on end arrows in (a). See context for details.

The charge correlation of two adjacent junction side strips is shown in Fig. 4. The negative channels mean that the output signals of the corresponding strip are negative. The negative signal is induced by the electron trapping effect, which has already been expatiated in Ref. [4, 8] and [10].

3.2 α-particles' energy spectrum and the CS effect of the ohmic side strips

The α-particles' energy spectrum from one ohmic side strip (for example the strip B4 in Fig. 1) is demonstrated in Fig. 5(a). One sharp peak (peak1) and one minor peak (peak2) are visible, in addition to a continuous background. Peak1 with energy resolution (FWHM) of $\sim$42 keV is the total energy peak induced by the 5.48 MeV α-particles stopped in the active region of the DSSSD. The correlation analysis of peak2 with junction side spectra shows that most of the selected events in peak2 (indicated by two up on end arrows in Fig. 5(a)) correspond to the low channel noise signals of the junction side strips. The illustration of this correlation analysis is similar to Fig. 3. This indicates that peak2 is induced by some of those α-particles that are stopped in the cross region 4 (see Fig. 1) of the DSSSD. The origin of peak2 in Fig. 5(a) and in Fig. 1) are the same. However, peak2 in Fig. 5(a) seems much more minor than that in Fig. 3. This happens because the signals from ohmic side strips do not participate in the Boolean logic operation of the trigger signal, so only a fraction of the α-particles that caused accidental coincident of the ohmic side signals with the noise signals of junction side strips are recorded.

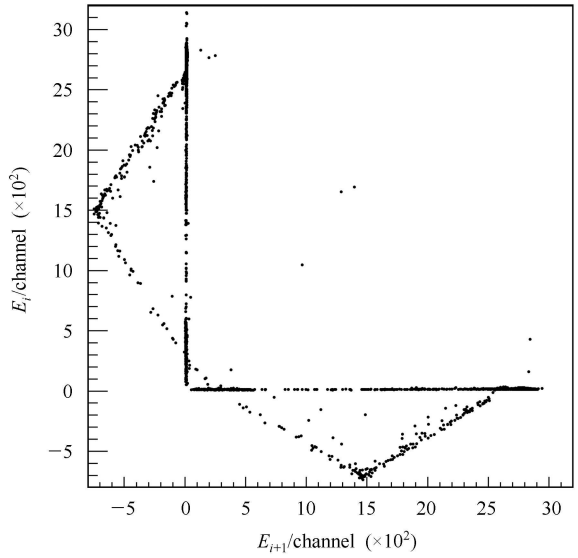

Fig. 4. Charge correlation between two adjacent junction side strips (strip i and i+1) while using ^{241}Am α source illuminate the junction side of the DSSSD. See context for details.

In the Fig. 5, the counts in the continuous background accounts for $\sim$30% of the counts of the whole spectrum. There are two sources for these continuous background events. One source is the CS events, as shown in Fig. 5(b), the other is the particles that are stopped in the junction side interstrip region, which induce the electron trapping effect and hence result in incomplete electron collection of the ohmic side strips [8]. This indicates that the cause of the continuous background is attributed to the particles stopping the inter-

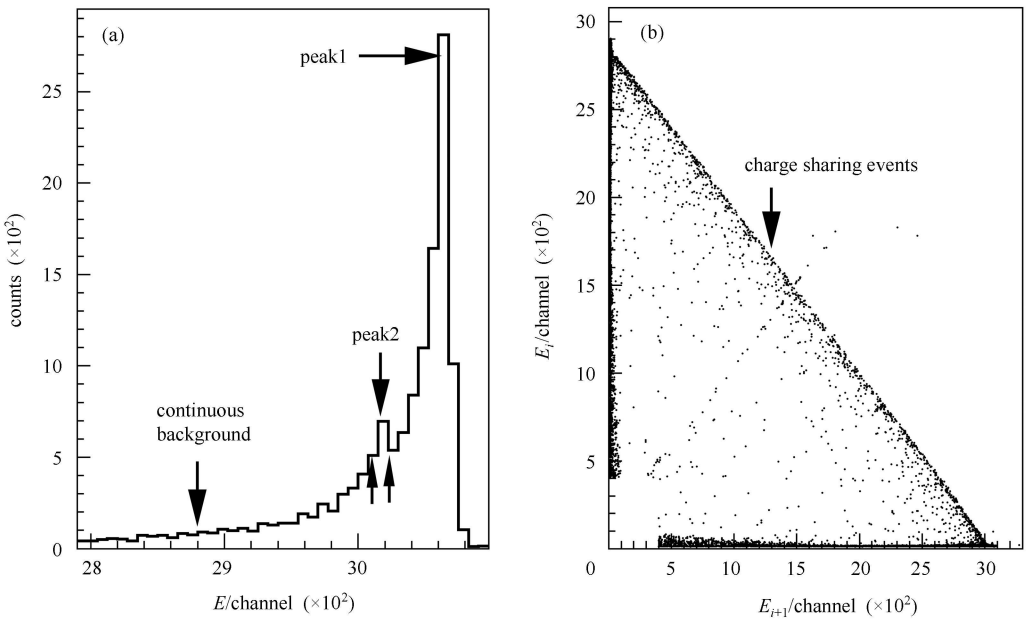

Fig. 5. (a) ^{241}Am α-particles' energy spectrum from one ohmic side strip, the two up on end arrows indicate the selected range of peak2 that used in the correlation analysis of the corresponding ohmic and junction side spectra. (b) Charge correlation between two adjacent ohmic side strips (strip i and i+1), the charge sharing (CS) events are presented as a line at constant E_i+E_{i+1}=$E_{\rm tot}$. See context for details.

strip area of both junction and ohmic sides. The summation of the area of the interstrip region on both junction and ohmic sides occupies ∼30% of the area of the DSSSD, and this percentage is consistent with the ratio of the number of counts in the continuous background to the counts in the whole spectrum.

The scatter plot of the charge correlation between two adjacent ohmic side strips is shown in Fig. 5(b). A typical charge sharing line at the constant E_i+E_{i+1}=$E_{\rm tot}$ is observed, which corresponds to the α-particles stopping in the cross region 1 (see Fig. 1) of the DSSSD. The number of counts of the CS events occupies ∼20% of the counts of the whole spectrum. This is consistent with the geometrical ratio between the area of the ohmic side interstrip and strip regions. These CS events contribute 2/3 of the counts of the continuous background, as shown in Fig. 5(a), and the other 1/3 is the contribution of these particles stopped in the junction side interstrip region.

4 Results of online test and analysis

Heavy ion beams with energies that can punch through the DSSSD are used to investigate the response of the detector working in transmission mode. The responses of the entrance face (junction side) and exit face (ohmic side) strips are reported and analyzed in this section.

In this test, the DSSSD and the SSD compose a ΔE-E telescope that is used for the particle identification. The experimental setup and the production of the heavy ion beams were reported in detail in Ref. [11].

4.1 Results of online test

Figure 6 shows a scatter plot of the charge correlation between two adjacent strips of the entrance face (a) and exit face (b), respectively. The CS events of the ohmic side strips show the same pattern as the result of the test with α source; that is, a line at constant E_i+E_{i+1}=$E_{\rm tot}$ is obtained. The surprising thing is that the entrance face strips' CS events give some raised events (see Fig. 6(a)) instead of a beeline. This will be interpreted in the next subsection.

Figure 7(a) is a typical experimental scatter plot of the ΔE-E telescope. The ΔE signal comes from one junction side strip of the DSSSD. Several absolutely separated belts accompanied with some contaminant are visible. Fig. 7(b) shows a ΔE spectrum of the selected events in the graphical cut cut_ELf in Fig. 7(a). The origination of the continuous background and peak2 (i.e. the contaminant of the ^{7}Be belt) will be expatiated infra.

Figure 8(a) is another typical scatter plot of the ΔE-E telescope. Here, the ΔE signal is form one exit face strip of the DSSSD. Fig. 8(b) shows the exit face ΔE spectrum. Comparing with Fig. 7(b), there is only one sharp peak (peak1) in Fig. 8(b) and some upper events appear. The cause of these upper events will be explained infra.

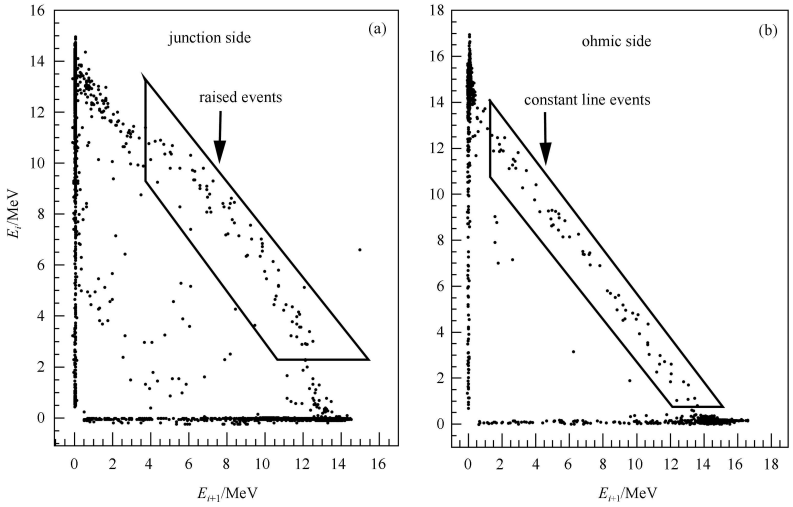

Fig. 6. Charge correlation between two adjacent strips (strip i and i+1) of entrance face (a) and exit face (b) in the test with heavy ion beams. Some of the charge sharing events are encircled by graphical cuts, and are marked as raised events in (a) and constant line events in (b). These two graphical cuts are examples of restrictive cuts used for correlation analysis of the ΔE spectra from entrance and exit face strips. See context for details.

4.2 Analysis of the online test results

Figure 6 shows the CS effect of the DSSSD working in the transmission model. CS events are observed on both junction side and ohmic side strips. These events are induced by those particles penetrating the corresponding interstrip gaps on both sides of the DSSSD [8]. So, the position information of these events can be recorded and the energy can be got by summing the energy values of the two adjacent strips. The raised events in Fig. 6(a) imply excess energy loss while particles punch through the junction side interstrip gaps. Except for these raised events, the other CS events of junction side strips exhibit a normal pattern that is the same as those constant line events in Fig. 6(b). This means that only a part of those particles that punch through the DSSSD from a position that very near to the junction side interstrip regions will induce excess energy loss. The cause of these raised events will be interpreted infra.

The response of one entrance face strip of the DSSSD working in transmission mode is shown in Fig. 7. Peak1 in Fig. 7(b) is the elastic scattering peak of the beam on the target [11].

The continuous background in Fig. 7(b) arises from the junction side CS events, as shown in Fig. 6(a). The ratio between the number of the counts in the continuous background and the counts of the whole ΔE spectrum is ∼10%. This is consistent with the geometrical ratio between the area of interstrip and strip regions of the junction side, which also confirms that the CS events originate from the junction side interstip region.

Peak2 in Fig. 7(b) represents the contaminant under each of the element belts in Fig. 7(a). It is clear that the ICC effect of the junction side strip results in the appearance of peak2; that is, the contaminant events in Fig. 7(a). The number of counts in peak2 after subtracting the included continuous background events occupy ∼20% of the counts of the whole ΔE spectrum. This leads to a hypothesis that these events in peak2 originate from particles punching through the DSSSD from cross region 1 (see Fig. 1), which occupies ∼20% of the area of the DSSSD. These ionising particles penetrating the DSSSD from cross region 1 will produce hole-electron pairs on its range. At the end of the track that is near to the interstrip gap of the ohmic side, the holes have a considerable probability of recombination because of the weak electric field of this region and the long route to the cathode [15, 16] (junction side strip); however, the electrons will be completely collected (by one or two adjacent strips of ohmic side) due to their high mobility. Correlation analysis is performed; that is, the CS events of ohmic side strips (see Fig. 6(b)) which originate from the interstrip region of ohmic side are used as restrictive cut to inspect the ΔE spectrum of junction side strip. The result, as shown in Fig. 7(b) with dashed lines, confirms that the events in peak2 of Fig. 7(b) are homologous with the CS events of the exit face strips; that is, these events originate from the particles punching through the DSSSD from cross region 1 (see Fig. 1). This validates the previous hypothesis on the origination of the peak2 in Fig. 7(b), and also indicates that the ohmic side interstrip gaps results in a strong ICC effect on the hole collection of the junction side strips while the DSSSD works in transmission mode. For these ICC events of junction side strips (i.e. the events in peak2 of Fig. 7(b)) the accurate energy values from junction side strip cannot be reconstructed; however, the position information is recorded without ambiguity.

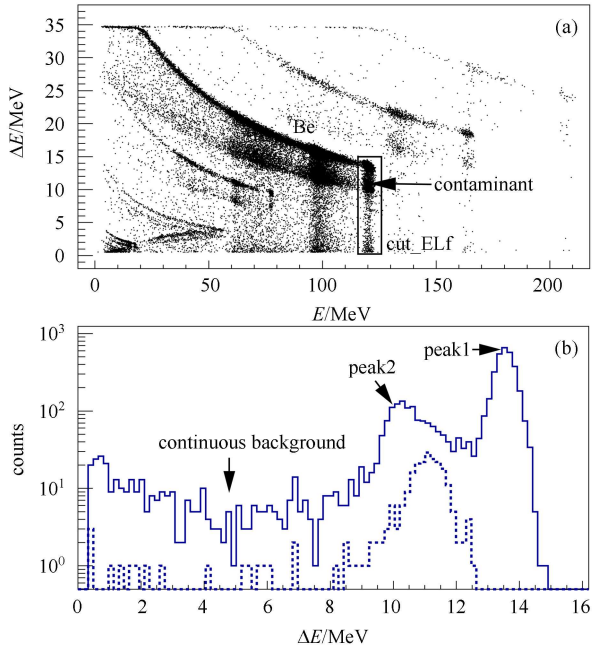

Fig. 7. (a)A typical scatter plot of the ΔE-E telescope. ΔE signal is from one entrance face strip of the DSSSD, E signal is from the SSD. The graphical cut named cut_ELf encircles those events used for the analysis. Some events with lower ΔE energies in the graphical cut cut_ELf are marked as contaminant, which represent these events under the element belts. (b) The solid line is the ΔE spectrum obtained by projecting the selected ^{7}Be events in the graphical cut cut_ELf to the Y-axis, and dashed line is the same ΔE spectrum with some restrictive graphical cuts from exit face strips as shown in Fig. 6(b) imposed. See context for details.

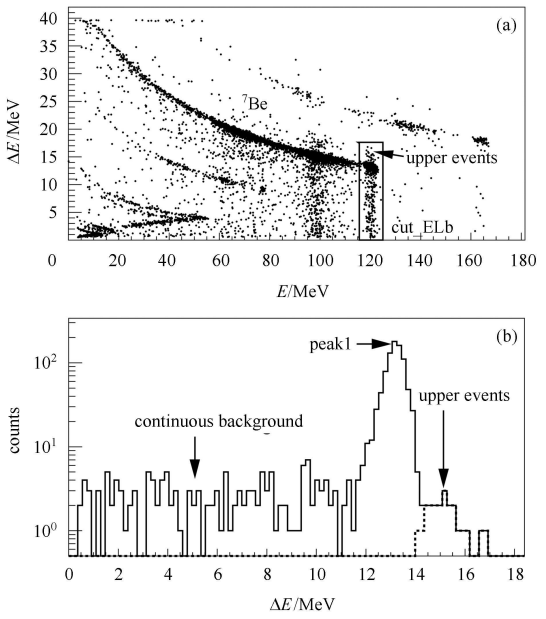

Fig. 8. (a) A typical scatter plot of the ΔE-E telescope. ΔE is from one exit face strip of the DSSSD, E is from the SSD. The graphical cut named cut_ELb encircled those events used for the analysis. Some events with higher ΔE energies in the graphical cut cut_ELb are marked as upper events. (b) The solid line is the ΔE spectrum obtained by projecting the selected ^{7}Be events in the graphical cut cut_ELb to the Y-axis, and dashed line is the same ΔE spectrum with some restrictive graphical cuts from junction side strips as shown in Fig. 6(a) imposed. See context for details.

Figure 8 shows the response of one exit face strip of the DSSSD working in transmission mode. Peak1 in Fig. 8(b) is the elastic scattering peak [11]. The continuous background in Fig. 8(b) comes from the CS events as shown in Fig. 6(b). The ratio of the number of the counts in the continuous background (i.e. the counts of CS events) to the counts of the whole spectrum is ∼15%. This means that the CS effect of ohmic side is reduced as compared with the result of the test using α source (see Fig. 5(b)), in which the ratio is consistent with the geometrical ratio between the area of ohmic side interstrip and strip regions; that is, 20%. The reduction of CS effect of ohmic side strips is related to the rise of the range of the particles in the DSSSD while illuminating its junction side [4].

The analysis of the online test result presents the energy and position information of the ICC and CS events, and ensures their validity as elastic scattering events [11]. As a typical example, the position distribution of the elastic scattering events of the ^{7}Be is shown in Fig. 9.

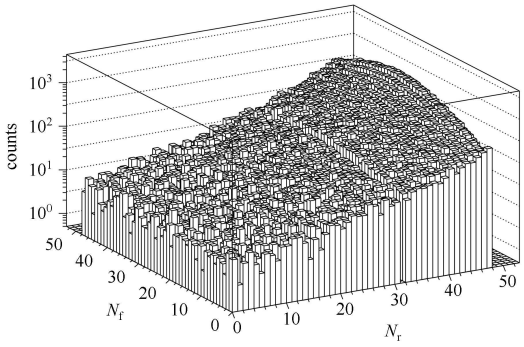

Fig. 9. 2D position distribution of the elastic scattering events. N_f and N_r is the strip number of the front and rear sides respectively.

The dashed line in Fig. 8(b) is the result of the correlation analysis of the upper events with the raised events in Fig. 6(a). The result shows that the upper events are homologous with these raised events showing in Fig. 6(a), which originates from the particles punching through the interstrip region of the junction side. This indicates that they have excess energy loss while the particles punch

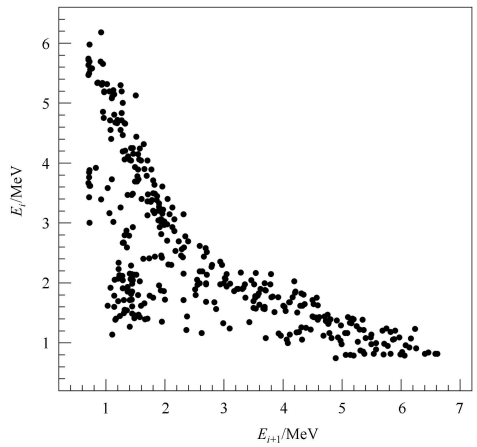

Fig. 10. Charge correlation between two adjacent junction side strips (strip i and i+1) of the DSSSD while the bias voltage is reduced.

through the junction side interstrip gaps. The excess energy loss is related to the structure of the DSSSD in the interstrip region of junction side; that is, the boundary structure of the junction side strips. It is found that if the bias voltage of the DSSSD is removed then the raised events will become sunken, as shown in Fig. 10. This implies that the depleted junction will extend underneath the interstrip gap of the junction side while an appropriate bias voltage is imposed upon the DSSSD, and hence the holes deposited in this region will be collected by the two adjacent junction side strips.

5 Summery

The performance of a DSSSD working in transmission mode is reported. The impacts of ICC and CS on the energy detection and position determination are evaluated by using short range α-particles from an ^{241}Am source and penetrating heavy ion beams illuminating the junction side of the DSSSD. The analysis shows that the energy information of CS events can be obtained by summing the energy signal of the two adjacent strips. In addition, the energy information of ICC events is deficient, and cannot be reconstructed. However, the position information of these events can be recorded without ambiguity, benefiting from the knowledge of the origination of these events.

We would like to express our appreciation to Prof. Z.K. Li (Institute of Modern Physics, Chinese Academy of Science) who made helpful comments on the manuscript.

References

1 Hall G. Reports on Progress in Physics, 1994, **57**(5): 481–531
2 Ostrowski A N, Cherubini S, Davinson T, Groombridge D, Laird A M, Musumarra A, Ninane A, Pietro A di, Shotter A C, Woods P J. Nucl. Instrum. Methods A, 2002, **480** (2–3): 448–455
3 Davinson T, Bradfield-Smith W, Cherubini S, DiPietro A, Galster W, Laird A M, Leleux P, Ninane A, Ostrowski A N, Shotter A C, Vervier J, Woods P J. Nucl. Instrum. Methods A, 2000, **454**(2–3): 350–358
4 Blumenfeld Y, Auger F, Sauvestre J E, Maréchal F, Ottini S, Alamanos N, Barbier A, Beaumel D, Bonnereau B, Charlet D, Clavelin J F, Courtat P, Delbourgo-Salvador P, Douet R, Engrand M, Ethvignot T, Gillibert A, Khan E, Lapoux V, Lagoyannis A, Lavergne L, Lebon S, Lelong P, Lesage A, Ven V Le, Lhenry I, Martin J M, Musumarra A, Pita S, Petizon L, Pollacco E, Pouthas J, Richard A, Rougier D, Santonocito D, Scarpaci J A, Sida J L, Soulet C, Stutzmann J S, Suomijärvi T, Szmigiel M, Volkov P, Voltolini G. Nucl. Instrum. Methods A, 1999, **421**(3): 471–491
5 Hutcheon D A, Bishop S, Buchmann L, Chatterjee M L, CHEN A A, D'Auria J M, Engel S, Gigliotti D, Greife U, Hunter D, Hussein A, Jewett C C, Khan N, Lamey M, Laird A M, LIU W, Olin A, Ottewell D, Rogers J G, Roy G, Sprenger H, Wrede C. Nucl. Instrum. Methods A, 2003, **498**(1–3): 190–210
6 Kemmer J. Nuclear Instruments and Methods, 1980, **169**(3): 499–502
7 Kemmer J. Nucl. Instrum. Methods A, 1984, **226**(1): 89–93
8 Yorkston J, Shotter A C, Syme D B, Huxtable G. Nucl. Instrum. Methods A, 1987, **262**(2–3): 353–358
9 Grassi L, Torresi D, Acosta L, Figuera P, Fisichella M, Grilj V, Jaksic M, Lattuada M, Mijatovic T, Milin M, Prepolec L, Skukan N, Soic N, Tokic V, Uroic M. AIP Conference Proceedings, 2012, **1491**(1): 135–136
10 Thomas Poehlsen, Eckhart Fretwurst, Robert Klanner, Sergej Schuwalow, Jörn Schwandt, Jiaguo Zhang. Nucl. Instrum. Methods A, 2013, **700**(0): 22–39
11 YANG Y Y, WANG J S, WANG Q, MA J B, HUANG M R, HAN J L, MA P, JIN S L, BAI Z, HU Q, JIN L, CHEN J B, Wada R, SUN Z Y, CHEN R F, ZHANG X Y, HU Z G, YUAN X H, CAO X G, XU Z G, XU S W, ZHEN C, CHEN Z Q, CHEN Z, CHEN S Z, DU C M, DUAN L M, FU F, GOU B X, HU J, HE J J, LEI X G, LI S L, LI Y, LIN Q Y, LIU L X, SHI F D, TANG S W, XU G, XU X, ZHANG L Y, ZHANG X H, ZHANG W, ZHAO M H, ZHANG Y H, XU H S. Nucl. Instrum. Methods A, 2013, **701**(0): 1–6
12 YANG Y Y, WANG J S, WANG Q, PANG D Y, MA J B, HUANG M R, HAN J L, MA P, JIN S L, BAI Z, HU Q, JIN L, CHEN J B, Keeley N, Rusek R, Wada R, Mukherjee S, SUN Z Y, CHEN R F, ZHANG X Y, HU Z G, YUAN X H, CAO X G, XU Z G, XU S W, ZHEN C, CHEN Z Q, CHEN Z, CHEN S. Z, DU C M, DUAN L M, FU F, GOU B X, HU J, HE J J, LEI X G, LI S L, LI Y, LIN Q Y, LIU L X, SHI F D, TANG S W, XU G, XU X, ZHANG L Y, ZHANG X H, ZHANG W, ZHAO M H, GUO Z Y, ZHANG Y H, XU H S, XIAO G Q. Physical Review C, 2013 **87**(4): 044613PRC
13 SUN Z, ZHAN W L, GUO Z Y, XIAO G, LI J X. Nucl. Instrum. Methods A, 2003, **503**(3): 496–503
14 Torresi D, Stanko D, Pietro A Di, Figuera P, Fisichella M, Lattuada M, Milin M, Musumarra A, Pellegriti M, Scuderi V, Strano E, Zadro M. Nucl. Instrum. Methods A, 2013, **713**(0): 11–18
15 Anokhin I E, Zinets O S. Nucl. Instrum. Methods A, 2002, **477**(1–3): 110–113
16 Livingston K, Woods P J, Davinson T, Shotter A C. Nucl. Instrum. Methods A, 1996, **370**(2–3): 445–451